Journal of The Korean Astronomical Society
37: 509 ∼ 515, 2004

SIMULATING NONTHERMAL RADIATION FROM CLUSTER RADIO GALAXIES

I. L. Tregillis[1], T. W. Jones[2], and Dongsu Ryu[3]
[1]Applied Physics Division, MS B259, Los Alamos National Laboratory, Los Alamos, NM 87545, U.S.A.
[2]School of Physics and Astronomy, University of Minnesota, Minneapolis, MN 55455, U.S.A.
[3]Department of Astronomy & Space Science, Chungnam National University, Daejon 305-764, Korea
E-mail: iant@lanl.gov, twj@msi.umn.edu, ryu@canopus.chungnam.ac.kr

ABSTRACT

We present results from an extensive synthetic observation analysis of numerically-simulated radio galaxy (RG) jets. This analysis is based on the first three-dimensional simulations to treat cosmic ray acceleration and transport self-consistently within a magnetohydrodynamical calculation. We use standard observational techniques to calculate both minimum-energy and inverse-Compton field values for our simulated objects. The latter technique provides meaningful information about the field. Minimum-energy calculations retrieve reasonable field estimates in regions physically close to the minimum-energy partitioning, though the technique is highly susceptible to deviations from the underlying assumptions. We also study the reliability of published rotation measure analysis techniques. We find that gradient alignment statistics accurately reflect the physical situation, and can uncover otherwise hidden information about the source. Furthermore, correlations between rotation measure (RM) and position angle (PA) can be significant even when the RM is completely dominated by an external cluster medium.

Key words : galaxies: jets – MHD – nonthermal radiation – radio continuum: galaxies

I. INTRODUCTION

Radio galaxies (RGs) play an important role in the study of large-scale magnetic fields. Not only do they constitute invaluable tools for studying cluster fields (*e.g.,* see the papers in these proceedings by Clarke and Johnston-Hollitt), but also there is mounting evidence that RGs directly influence the evolution of large-scale fields (*e.g.,* Nulsen et al., 2002, see also the paper by Li in these proceedings). Critically evaluating the observational analyses used to characterize RG magnetic fields is therefore a valuable exercise.

Detections of inverse-Compton scattered cosmic microwave background photons (hereafter IC/3K emission) can be combined with radio synchrotron observations to extract information about RG magnetic fields (e.g., Harris & Romanishin, 1974; Cooke, Lawrence, & Perola, 1978; Harris & Grindlay, 1979). An alternative method for deriving field values makes use of minimum-energy (ME) arguments. This is useful when X-ray observations are unavailable, although conclusive theoretical arguments for equipartition between radio-emitting electrons and magnetic fields remain elusive.

Both field measurements require assumptions about the particle and field distributions, such as volume filling factors, spectral cutoffs, and other parameters that are not directly accessible to observations. Furthermore, the standard IC/3K and ME calculations are based on a uniform magnetic field geometry and a pure powerlaw distribution of particles. Yet these assumptions are highly unrealistic in many situations.

Rotation measure (RM) maps of extragalactic radio sources fall prey to similar difficulties, because often the distribution of thermal magnetoionic plasma (the "Faraday screen") is unobservable. While most RM data support the notion of a Faraday screen that is physically distinct from the synchrotron-emitting lobe plasma, uncertainties in the character of the Faraday medium can lead to vexing ambiguities. For instance, one question is whether systematic surveys of cluster RM values suffer contamination from background galaxies (Rudnick & Blundell, 2003; Ensslin, Vogt, Clarke, & Taylor, 2003).

Synthetic observations are an ideal tool for investigating these issues. The technique combines minimal use of simplifying assumptions with complete knowledge of the actual physical conditions in the source.

II. NUMERICAL METHODS

Our numerical methods have been detailed in Jones, Ryu, & Engel (1999), Tregillis, Jones, & Ryu (2001), and Tregillis, Jones, & Ryu (2004) (hereafter TJR04). We refer the reader to those papers for a complete description. In short, we follow the bulk flow through a three-dimensional total variation diminishing (TVD) Eulerian ideal MHD scheme. Within the nonrelativistic bulk MHD flows, we evolve a passive population of relativistic electrons ($E_e \leq 10$ GeV) through the standard particle kinetic equation. The particle evolution is treated self-consistently, incorporating first-order Fermi acceleration at shocks as well as adiabatic

Proceedings of The 3rd Korean Astrophysics Workshop on
Cosmic Rays and Magnetic Fields in Large Scale Structure

and radiative cooling.

(a) The Models

The passive nature of the nonthermal electron populations enabled us to conduct several numerical simulations of the same dynamically-identical jet, each focused on a different set of cosmic ray (CR) parameters. The dynamical model consisted of a light ($\rho_{jet}/\rho_{amb} = 10^{-2}$), supersonic ($M_{jet} = 8$), magnetized ($B_\phi = 2B_{x0}(r/r_j)$ for $r \leq r_j$) jet propagating through a uniform ambient magnetized medium ($B_{amb} = B_x = B_{x0}$). The jet was not magnetically dominated, with $\beta = 10^2$ initially on axis.

Radiative cooling timescales (τ_{rad}) were parameterized through the physical value of B_{x0}. The injection of fresh nonthermal particles at shocks was parameterized via the parameter ϵ, the fraction of the thermal flux through each shock injected into the downstream nonthermal population. Parameter values for all three models are listed in Table (a).

Table 1
Summary of Simulations

Model	ϵ	B_{xo} (μG)	τ_{rad}/τ_{end}
Control (1)	0.0	0.39	1.6×10^3
Injection (2)	10^{-4}	0.39	1.6×10^3
Cooling (3)	0.0	5.7	1.0

In each model, the jet nonthermal electron population entered with a momentum index $q = 4.4$, representing a synchrotron spectral index, $\alpha = (q-3)/2 = 0.7$, where $S_\nu \propto \nu^{-\alpha}$.

(b) Synthetic Observations

We synthetically observe the simulated jets as follows. First, we combine vector magnetic field and nonthermal electron distribution data to calculate self-consistent synchrotron radio and IC/3K X-ray volume emissivities in every zone of the computational grid. Then we apply a ray-casting procedure to perform line-of-sight (LOS) integrations and project the simulated objects on the sky. The output is written in FITS format and analyzed using conventional packages (MIRIAD and KARMA (Gooch, 1995)).

As given by Jones, O'Dell, & Stein (1974) (hereafter JOS), the synchrotron emissivity is

$$j_s(\nu) = j_{\alpha 0} \frac{4\pi e^2}{c} f(p_s) p_s^q \left(\frac{\nu_{B_\perp}}{\nu}\right)^\alpha \nu_{B_\perp}. \qquad (1)$$

The spectral index α is related to the local electron momentum index q via $\alpha = (q-3)/2$, $\nu_{B_\perp} = eB \sin\Omega/(2\pi m_e c)$, where Ω projects the local field onto the sky, and $j_{\alpha 0}$ is a dimensionless constant, defined in JOS. For a selected observing frequency, ν, the distribution, $f(p_s)$, and the index, q, are determined for each point on the grid by establishing the relevant electron momentum from the relation $p_s = [2\nu/(3\nu_{B_\perp})]^{(1/2)}$, with p_s in units $m_e c$. This calculation properly accounts for spectral curvature and the orientation of the magnetic field on the plane of the sky.

The X-ray IC/3K emissivity, $j_{3K}(\nu_X)$, can be simply expressed at a selected X-ray frequency, ν_X, in terms of the synchrotron emissivity, $j_s(\nu_X)$, in Eq. (1) extrapolated to ν_X; namely (JOS)

$$j_{3K}(\nu_X) = e^{3K}_{\alpha 0} \frac{\sigma_T c}{e^2} \frac{c u_\mu \nu_\mu^{\alpha-1}}{4\pi \nu_{B_\perp}^{1+\alpha}} (1+z)^{3+\alpha} j_s(\nu_X) , \qquad (2)$$

where $u_\mu = aT_0^4$ and $\nu_\mu = kT_0/h$ are the energy density and characteristic frequency, respectively, at the current epoch of the CMB, while $e^{3K}_{\alpha 0}$ is another order-unity constant defined in JOS. We note that $j_s(\nu_X)$ is normalized and α is determined at $p_\mu = (\nu_X/\nu_\mu)^{1/2}$.

We calculate the Faraday rotation (FR) along the line of sight to each zone, $d\chi(L)$, via

$$d\chi(L) = \frac{e^3}{2\pi m_e^2 c^2 \nu^2} \int_0^L n_{th}(l)\ B_\parallel(l)\ dl\ . \qquad (3)$$

$B_\parallel$ is the component of the magnetic field parallel to the line of sight, and n_{th} is the thermal particle number density in each zone. This integration is performed separately for each zone, and only along the portion of the line of sight from the edge of the computational grid to that zone (located at distance L from the edge). Once $d\chi$ is known for every zone, we also construct the Faraday-rotated Stokes parameters:

$$Q2_s(\nu) = \int \Pi(\alpha)\ j_s(\nu)\ \cos[2(\chi + d\chi(l))]\ dl \qquad (4)$$

$$U2_s(\nu) = \int \Pi(\alpha)\ j_s(\nu)\ \sin[2(\chi + d\chi(l))]\ dl \qquad (5)$$

Here χ is the angle of the magnetic field within that zone projected on the plane of the sky, and $\Pi(\alpha)$ is the synchrotron fractional polarization in that zone. We take $\Pi(\alpha)$ as $(\alpha+1)/(\alpha+\frac{5}{3})$, corresponding to the value predicted for a locally uniform field.

III. FIELD STRENGTH ESTIMATES

Magnetic field strength can be calculated very simply from synchrotron and IC/3K intensities for a uniform medium when the electron distribution is a powerlaw. We used the following expression for this estimated field, B_{ic} in μG (e.g., JOS, Harris & Romanishin, 1974; Harris & Grindlay, 1979):

$$B_{ic}^{1+\alpha} = (1.06 \times 10^{-11})\ (2.09 \times 10^4)^{\alpha-1} \left(\frac{j^{3K}_{\alpha 0}}{j_{\alpha 0}}\right) \times (1+z)^{3+\alpha} \left(\frac{\nu_r}{\nu_X}\right)^\alpha \frac{I_S(\nu_r)}{I_{3K}(\nu_X)}\ . \qquad (6)$$

For uniform particle and field distributions, this expression is exactly equivalent to inverting the analytic calculation of synchrotron and IC/3K surface brightnesses in our synthetic observations.

Similarly, the standard expression used to compute the minimum-energy magnetic field, B_{me}, in Gauss is (Miley (1980)):

$$B_{me} = 5.69 \times 10^{-5} \left[\frac{\nu_2^{1/2-\alpha} - \nu_1^{1/2-\alpha}}{(1/2-\alpha)} \right]^{2/7} \times \left[\left(\frac{1+k}{\eta} \right) \frac{F(\nu_r)}{\nu_r^{-\alpha}} \frac{(1+z)^{3+\alpha}}{\theta_x \ \theta_y \ \ell \ \sin^{3/2}\vartheta} \right]^{2/7} . \quad (7)$$

Here $F(\nu_r)$ is the observed radio flux density within an observing beam, $k \equiv U_{proton}/U_E$, η is a magnetic field volume filling factor, ϑ is the angle between the magnetic field and the line of sight, θ_x and θ_y are the semimajor and semiminor axes of the observing beam in arcseconds, ℓ is the path length through the source in kpc, and ν_1 and ν_2 are the *fixed* lower and upper synchrotron cutoff frequencies in the source frame, expressed in GHz. We assume below for simplicity that $k = \eta = \sin\vartheta = 1$. The magnetic field is so tangled and intermittent that assuming $\sin\vartheta = 1$ introduces errors of only a few percent into our analysis.

In order to incorporate the full nonthermal electron distributions as well as possible into B_{me}, the frequency limits in Eq. (7) correspond in each model to the characteristic synchrotron frequencies of the lowest and highest energy electrons and the fiducial magnetic field for each model. Those turn out to be $\nu_1 = 100$ Hz and $\nu_2 = 30$ GHz for the Control and Injection models; for the Cooling model, $\nu_1 = 1500$ Hz and $\nu_2 = 450$ GHz. Our conclusions do not depend on any of these parameter choices.

Our analysis is summarized in Fig. 1, which compares B_{ic} and B_{me} to B_{rms} for the same six LOS in each model. The LOS were chosen to sample a variety of physical and spectral structures. The details of the selections are given in TJR04.

Both empirical field estimates correlate roughly with B_{rms} along the selected lines of sight. The bolometric synchrotron intensity does depend on the rms magnetic field along the line of sight, of course. The spectral emissivity $j_s(\nu) \propto B^{1+\alpha}$, is similar, since in our sources spectral index values in the range $\alpha \sim 0.7 - 1$ are common. Still it is not obvious a priori how well such a simple measure as B_{rms} should compare to inferred values, so the experiment is valuable. Two-thirds of the B_{ic} (B_{me}) points are within a factor of two (three) of B_{rms}. The B_{ic} values are approximately randomly distributed with respect to B_{rms}.

LOS 6 passes through the jet near its origin. At that location, the field structure is relatively simple and approximates that introduced at the computational boundary. Furthermore, the emission is dominated by young electron populations that have not yet experienced strong radiative aging. B_{ic} is very close to B_{rms} at this location in all three models.

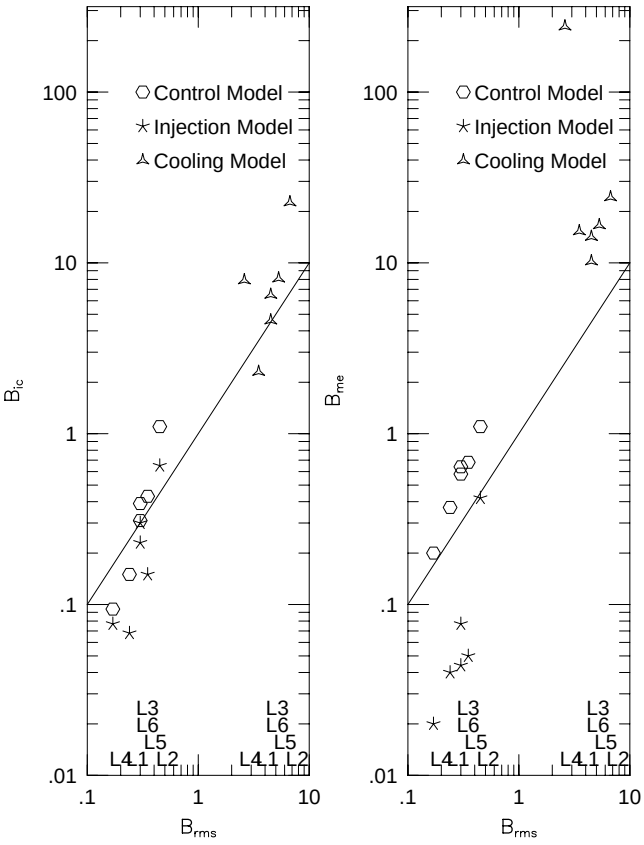

Fig. 1.— Comparisons of magnetic field measures. Symbols indicate the electron transport model. Associated line-of-sight numbers are marked at the bottom of each plot according to the associated B_{rms} values. From Tregillis, I. L., Jones, T. W., & Ryu, D. 2004, ApJ, 601, 778.

Lobe values of B_{ic} (e.g., LOS 1 and 4) tend to fall below B_{rms}. This bias results from the presence of substantial electron populations in weak field regions that contribute little to the radio emission, but that do produce X-rays. In effect the IC/3K intensity provides an overestimate of the number of radio emitting electrons, so that under the uniform source hypothesis the field required to account for the radio emission is weakened. When compared to the distribution of field values along individual LOS, B_{ic} is generally representative of the values being sampled. Thus it does give a "meaningful" result, if not a simply defined quantitative one.

Notable exceptions occur in the presence of strong spectral curvature, such as along LOS 4 in the cooling model. Intentionally, no correction was made for the convex spectrum at this location, in order to expose its potential influence. The 1.2 keV IC/3K emission used to compute B_{ic} comes from 1 GeV electrons, while the 2.9 GHz emission is produced by electrons with energies about an order of magnitude higher, even in the

strongest field regions along this LOS. A convex electron spectrum will artificially increase B_{ic}, as simple arguments can show.

Suppose, for example, we measured the bolometric synchrotron intensity, I_S, from electrons of energy γ_S and the bolometric IC/3K intensity, I_{3K}, from electrons of energy γ_{3K}. For a homogeneous source and fixed radio band, it is simple to show that $B \propto (I_S/I_{3K})N_{\gamma_{3K}}/N_{\gamma_S}$, where $N_{\gamma_{3K}}$ and N_{γ_S} represent the number of electrons required to produce the observed intensities. If we assumed a γ powerlaw between $N_{\gamma_{3K}}$ and N_{γ_S} with index determined by the energetic electrons responsible for the radio emission,we would overestimate B when the distribution is actually convex, since we would overestimate $N_{\gamma_{3K}}/N_{\gamma_S}$.

The impact of curvature is even more striking on the value of B_{me} for LOS 4 in the cooling model. Under the equipartition that accompanies the minimum energy assumption, the effective overestimate of the electron population also exaggerates the estimated magnetic field energy, leading to a field value about two orders of magnitude greater than B_{rms} and even an order of magnitude greater than B_{max} along this LOS.

Our simulated objects are not in particle/field equipartition, nor is there physics in the simulations expected to produce this kind of equipartition. Thus, while B_{ic} errors are randomly distributed with respect to B_{rms}, there are obvious biases in the relationship between B_{me} and B_{rms}. Those biases correctly reflect actual deviations from the minimum energy condition. In short, they trace the relationship between nonthermal particle and magnetic field energies in the predominant emission regions.

B_{ic} and B_{me} can be combined to obtain a purely observational measure of the particle/field energy partitioning, regardless of how far out of equipartition the emission region might be. Details are given in TJR04.

IV. STRUCTURAL DEPOLARIZATION

Synthetic observations are useful when examining observationally-inferred field topologies, because we know the entire three-dimensional field from the numerical simulation data.

Laing (2002) has derived expressions for the total and polarized intensity from a powerlaw electron distribution in an anisotropic and disordered magnetic field, based on an earlier treatment by Matthews & Scheuer (1990). In this treatment, the field is assumed to have been generated by compression and shearing of an initially isotropic Gaussian distribution of field components with zero mean. The Laing (2002) treatment is particularly nice because the expressions have only one free parameter, the ratio of the RMS values of the two field components on the plane of the sky:

$$\Upsilon \equiv \frac{B_{\perp_1}^{RMS}}{B_{\perp_2}^{RMS}} \tag{8}$$

(note that Laing uses η for this quantity).

Given the simplicity of the Laing (2002) treatment, checking those results against our synthetic polarimetry data is very straightforward. Spectra in the Control Model are powerlaw everywhere, and the local spectral index α is very nearly constant throughout the volume of that simulation, making it particularly well-suited to this treatment. At a given location on the source, we can use the synthetically-observed fractional polarization to invert the Laing (2002) results and derive a theoretical value for Υ from the Laing formulation. We can also calculate Υ directly from the magnetic field along each line of sight. The field distribution carried down the jet in our simulations is decidedly non-Gaussian, though the initial fields are highly uniform; thus, this comparison is a useful test of the accuracy of Laing's field description in less idealized circumstances.

Table 2
Predicted and Measured Υ Values

m	LOS	Υ_{Laing}	$\Upsilon_{simulation}$
0.691	2	0.12	0.96
0.681	3	0.15	0.35
0.660	5	0.19	0.40
0.613	1	0.26	0.61
0.579	6	0.30	0.88
0.150	4	0.80	0.95

Table IV lists the Υ values obtained at several locations on the source by inverting the calculation of Laing (2002, Eq. (12) and (13)) and directly from the simulation data. Overall, the two Υ values show little agreement and some striking disagreement. The Laing model predicts $m \to 0$ as $\Upsilon \to 1$, which is quite reasonable under the assumptions of that model. We see that the simple monotonic scaling is not preserved in more complex environments.

This is convincingly illustrated by comparison of the lines of sight 2 and 4, which are the locations of the highest and lowest fractional polarizations of the lines sampled. LOS 4 lies on a region of very low fractional polarization, $m = 0.15$. The theoretical prediction based on Gaussian field distributions sets $\Upsilon = 0.80$, while the value in the simulated object is $\Upsilon = 0.95$. These values are qualitatively consistent with each other, and the notion that two orthogonal field components of nearly equal strength should give rise to little polarized emission.

Yet that argument severely underestimates the effect of field nonuniformity, a point made abundantly clear by the values on line 2. The fractional polarization at line 2, $m = 0.69$, is close to the maximum for $\alpha = 0.70$; the theoretical Gaussian calculation therefore predicts a low value for Υ, namely, $\Upsilon = 0.12$. Yet, the actual value in the code is effectively the same as that on LOS 4: $\Upsilon = 0.96$.

As described in TJR04, LOS 2 passes through the plasma just downstream of a strong terminal jet shock, evidenced by an extremely sharp peak in the line-of-sight magnetic field distribution. This is, accordingly, one of the brightest locations on the source. Most of the emission, and also most of the polarized emission, is dominated by a very small region along the line of sight. This region consists of jet plasma which has been strongly shocked, and therefore harbors a highly-ordered magnetic field. Yet most of the magnetic field along the line of sight lies in the lobe, where the field is highly disordered. Thus the calculation of Υ along the line of sight, which is not emission weighted, indicates a highly disordered field, with $\Upsilon \approx 1$. The description of the source magnetic field distribution as the distortion of an initially Gaussian distribution does not adequately describe such sharp nonuniformities in the field. When the RMS fields are computed only over the portion of the line of sight associated with the extreme hotspot field spike, the Υ drops to $\Upsilon = 0.29$, closer to the Laing value.

While most extreme at LOS 2, this appears to be a general feature of the two Υ calculations. The values obtained directly from the simulation data tend to be higher than those indicated by the Laing model, indicating more highly disordered fields. The Laing model may provide a useful lower bound for the degree of field disorder.

V. ROTATION MEASURE DIAGNOSTICS

We construct RM maps of our simulated sources from multifrequency synthetic polarimetry datasets. We note that since FR depends only on the thermal density and magnetic field strength, RM maps for the three dynamically-identical models differ only in overall scale factors. Thus in this section we restrict our attention to the Control Model.

Rudnick & Blundell (2003) have suggested using scatterplots of RM versus position angle (PA) to identify local and nonlocal Faraday screen contributions. The statistical distribution of points in the RM/PA plane can identify biases created by interactions of a local Faraday screen with an extragalactic radio source. Conversely, uncorrelated RM and PA fluctuations might arise when the bulk of the FR occurs far away from the radio source (where information about the PA distribution originates), such as along the long lines of sight through a cluster.

Ensslin, Vogt, Clarke, & Taylor (2003) put forward a more rigorous quantitative analysis of the RM/PA plane. For this purpose they introduced a pair of scalar statistics calculated from the gradients of the RM and PA distributions: an alignment statistic, A, and a vector product statistic, V. A complete description and analysis of both statistics is given in Ensslin et al. (2003). For our purposes it suffices to note that $A + V$ values near unity indicate strong correlation, and values near zero indicate a low degree of correlation.

Synthetic polarimetry observations are particularly well-suited to an RM/PA analysis. Scatterplots derived from real-world RM datasets can potentially be constructed from two separate sets of PA values, because the RM data can be plotted against either the original (uncorrected) PA values or the Faraday-corrected PA values. Synthetic observations provide a third option. By turning off FR in the radiative transfer calculations, we can obtain the "true" PA distribution on the source, as opposed to the Faraday-corrected values. Ideally, these two sets of values would be identical after applying a perfect derotation. Thus synthetic polarimetry provides a useful tool for identifying systematic errors in map correction algorithms.

We begin by calculating the gradient alignment statistics for a "naked" source, where the contributions from all external media have been filtered out. This is an important experiment that can only be performed through simulations. (In real sources the much higher thermal density of the displaced ambient medium will create a "skin" surrounding the lobe with a significantly higher Faraday depth than through the lobe itself, even for low levels of magnetization. This is the case in our simulations even without the presence of an extended cluster medium.) In this situation the FR takes place entirely within the source, in the same synchrotron-emitting plasma where the PA data originate. Thus the physical situation guarantees that the RM and PA distributions will be highly correlated. We therefore require the gradient alignment statistics to indicate the existence of such a correlation. And, indeed, in this case the gradient alignment calculation returns $A = 0.986$, $V = -0.065$, and $A + V = 0.921$, consistent with strong correlation.

Next we examine the gradient alignment statistics when the contribution from the Faraday skin is included. Here we include only the disturbed ambient medium immediately surrounding the radio source. This experiment is still only possible with synthetic observations, because it purposely excludes potential contributions from undisturbed or unrelated material along the very long line of sight between the observer and the source (such as through a cluster). Now the bulk of the FR takes place in a thermal plasma disparate from the synchrotron emitting regions where the PA data originate. Thus we expect the RM/PA correlation to be diminished. But note that the Faraday skin interacts with and is shaped by the expanding radio lobe, creating a dynamical relationship between the synchrotron plasma where PA data originate and the thermal plasma where the FR takes place. This might maintain a lower level of correlation, weaker than in the case of the "naked" radio lobe. The gradient alignment statistics return $A = 0.977$, $V = -0.071$, and $A + V = 0.906$, consistent with our expectations.

In these models the skin has fairly uniform Faraday depth, because the original undisturbed ambient medium has a uniform thermal density and field geometry. In this case it acts largely as an offset in the RM

without introducing large variations across the source, so the correlation is only slightly diminished. A nonuniform environment could lead to more variations in the skin and hence a lower $A + V$ value, depending on the scale size of the fluctuations (see below).

After verifying that the gradient alignment statistics give sensible results for calculations on "clusterless" RM maps, we examined the effect of an external cluster medium on these calculations. For these experiments it was not necessary to include an extended cluster environment in our numerical RG simulations, nor was it necessary to use data generated in structure-formation calculations. Since we were solely interested in the cluster environment strictly as a Faraday medium, we simply generated Faraday screens representing clumpy, randomized distributions of a magnetoionic medium with different RMS Faraday depths. For each synthetic cluster screen we used a line-of-sight path length of 1 Mpc, a characteristic thermal density $n_{th} = 10^{-3}$ cm^{-3} and a characteristic field strength $B_{\parallel} = 1\mu$G. We assumed that the clusters contain no synchrotron-emitting plasma. Random generation virtually guarantees that the screen fluctuations are completely independent of the physical structures in our numerical models.

Characteristic RM values for the control model with the Faraday skin in place are on the order of 10 rad/m^2. The low values are caused by the extremely low physical magnetic field scale used to suppress radiative cooling as explained above. (Cooling model RM values are larger by a factor of 3200, putting them in a regime consistent with numerous observations of extragalactic radio sources.) The RM contributions from the cluster screens themselves range from 320 to 2.4×10^4 rad/m^2. Thus in every case the RM is completely dominated by the cluster screen.

The effect of the cluster screen on the RM/PA plane is illustrated in Fig. 2. The left-hand panel shows the RM/PA scatterplot for the control model with the Faraday skin in place but no external cluster medium. There is a fair amount of fine structure in the plot, indicative of the strong correlation we obtained above. The right-hand panel shows the same plot when the FR includes the contribution from a cluster screen with 5″ angular fluctuation scale. We see that the RM values are now significantly larger, but most of the fine structure obvious to the naked eye has been washed out. The following experiment demonstrates that the naked eye is an unreliable tool for uncovering correlations.

Table V shows the variation in A and V values as a function of the angular scale for correlations in the randomly-generated external cluster environment. The correlation $(A + V)$ drops significantly once the fluctuation length scale drops below approximately 2.5″. RM maps of the simulated sources without an external cluster medium exhibit coherent fluctuations on scales ranging from roughly 3″ to 20″. Thus fluctuations in the cluster environment begin to wash out lo-

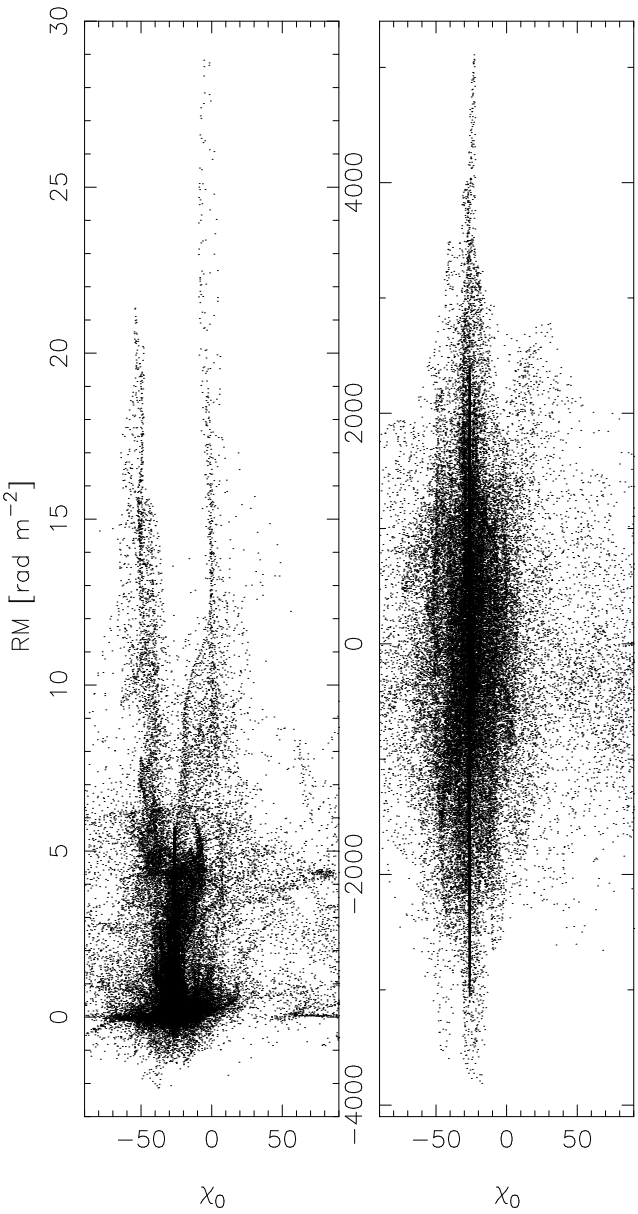

Fig. 2.— RM/PA scatterplots for the control model. Left: Faraday skin present, but no contribution from an extended cluster medium. $A + V = 0.906$ for this plot, consistent with the high degree of fine structure present. Right: Faraday skin present, and FR includes contribution from cluster Faraday screen with 5″ fluctuation scale and $\left\langle \left(n_{th} B_{\parallel}\right)^2 \right\rangle^{1/2} = 2.8 \times 10^{-3}$. $A + V = 0.791$ for this plot.

TABLE 3
GRADIENT ALIGNMENT STATISTICS

Patch size	$\left\langle \left(n_{th} B_{\parallel}\right)^2 \right\rangle^{1/2}$	A	V	$A+V$
$0.5''$	2.98×10^{-2}	0.003	0.034	0.037
$1.0''$	1.46×10^{-2}	0.429	-0.107	0.322
$2.5''$	5.69×10^{-3}	0.915	0.102	1.02
$3.0''$	4.71×10^{-3}	0.900	0.102	1.00
$5.0''$	2.80×10^{-3}	0.749	0.042	0.791
$10.0''$	1.38×10^{-3}	0.850	-0.016	0.834
$15.0''$	9.06×10^{-4}	0.912	0.023	0.935
$30.0''$	3.92×10^{-4}	0.956	0.099	1.06

cal RM/PA correlations when the angular scale of the cluster fluctuations approaches that of fluctuations on the Faraday skin surrounding the radio galaxy. This demonstrates that meaningful information about the angular size of coherent patches on the "naked" radio galaxy is embedded in the RM/PA gradient alignment statistics.

More significantly, we see that large cluster contributions to the FR do not necessarily eliminate RM/PA correlations, and might even introduce new ones. Thus the existence of RM/PA correlations in cluster RM samples is not conclusive evidence for a local origin to the FR.

ACKNOWLEDGEMENTS

The work by I.L.T. and T.W.J. was supported by the NSF under grants AST96-16964 and AST00-71176 and by the University of Minnesota Supercomputing Institute. The work by D.R. was supported in part by KOSEF through grant R01-2004-000-10005-0. We gratefully acknowledge Larry Rudnick, Robert Laing, and Torsten Ensslin for helpful discussions.

REFERENCES

Clarke, T. E. 2004, these proceedings

Cooke, B. A., Lawrence, A., & Perola, G. C. 1978, MNRAS, 182, 661

Ensslin, T., Vogt, C., Clarke, T. E., & Taylor, G. B. 2003, ApJ, 597, 870

Gooch, R. E. 1995, in ASP Conf. Ser. 101, Astronomical Data Analysis Software and Systems V, ed. G. H. Jacoby & J. Barnes (San Francisco: ASP), 80

Harris, D. E. & Grindlay, J. E. 1979, MNRAS, 188, 25

Harris, D. E. & Romanishin, W. 1974, ApJ, 188, 209

Johnston-Hollitt, M. 2004, these proceedings

Jones, T. W., O'Dell, S. L., & Stein, W. A. 1974, ApJ, 188, 353 (JOS)

Jones, T. W., Ryu, D., & Engel, A. 1999, ApJ, 512, 105

Laing, R. A. 2002, MNRAS, 329, 417

Li, H. 2004, these proceedings

Matthews, A. P. & Scheuer, P. A. G. 1990, MNRAS, 242, 623

Miley, G. 1980, ARA&A, Vol. 18 (Annual Reviews, Inc.), 165

Nulsen, P. E. J., David, L. P., McNamara, B. R., Jones, C., Forman, W. R., & Wise, M. 2002, ApJ, 568, 163

Rudnick, L. & Blundell, K. 2003, ApJ, 588, 143

Tregillis, I. L., Jones, T. W., & Ryu, D. 2001, ApJ, 557, 475

Tregillis, I. L., Jones, T. W., & Ryu, D. 2004, ApJ, 601, 778 (TJR04)